

# Flood Risk Index Mapping utilizing Google Earth Engine technology: A Case Study on Taiwan

1<sup>st</sup> Wen-Hsin Chen

*College of Engineering*

*University of Missouri - Columbia*

Columbia, United States

mch84@missouri.edu

2<sup>nd</sup> Hatef Dastour

*MU Institute for Data Science and Informatics (MUIDSI)*

*University of Missouri - Columbia*

Columbia, United States

hdastour@missouri.edu

3<sup>rd</sup> Chi-Ren Shyu

*MU Institute for Data Science and Informatics (MUIDSI)*

*University of Missouri - Columbia*

Columbia, United States

shyuc@missouri.edu

**Abstract**—In recent years, the severity and frequency of natural disasters have been amplified by climate change, with global warming contributing to heavier rainfall events in Taiwan. The trend of increased rainfall intensities are reflected in phenomenon such as the tropical storm Lupit in August 2021 [1], the third-highest recorded rainfall in Taiwan’s history in January and February in 2022 [2], and rainfall levels during typhoon season that can reach 1000-1600 millimeters per day—an unprecedented intensity compared to previous decades [3]. The objective of this study was to address Taiwan’s growing flood risk by developing a flood risk index using Google Earth Engine Javascript and recent open-source satellite and statistical datasets. The values combined to form a comprehensive risk index followed the World Health Organization (WHO) recommended framework for calculating disaster risk. The methodology combined hazard, exposure, and vulnerability in the form of flood-specific geospatial factors such as flood inundation depth for return period, population density, soil composition, and other variables. The resulting flood risk map of Taiwan can help inform researchers and policymakers on how to prioritize flood mitigation infrastructure and services in the future. The related project files can be found on GitHub.

**Index Terms**—flood risk, Taiwan, risk classification, satellite data, disaster preparedness, Google Earth Engine

## I. INTRODUCTION

Shifting climate conditions have led to more frequent and intense rainfall events in Taiwan in recent years. Traditional approaches using historical flood observations are no longer sufficient to capturing the evolving and interconnected interactions that influence flood behavior. Despite this, in Taiwan, flood inundation maps are commonly used to identify risk and highlight size and depth of flooding. However, findings from semi-structured interviews with 14 stakeholders in flood management—from academia, government, and local communities—revealed the limitations of flood inundation maps provided by both the central agency and city-level government [4]. Many maps lack considerations of storm surge, rainfall, socioeconomic disparities, and distinct characteristics between urban and rural areas when depicting flood risk.

The shortcomings of Taiwan’s flood inundation maps stress the need for comprehensive flood risk classification maps that integrate factors such as population densities, land use patterns, and socioeconomic differences. The development of these maps can help improve infrastructural resilience and flood preparedness for a wider demographic in Taiwan.

To address these challenges, this study develops a flood risk index for Taiwan using Google Earth Engine Javascript and recent open-source satellite and statistical datasets. The index follows the World Health Organization’s recommended disaster risk framework, connecting hazard, exposure, and vulnerability into a unified classification map. By integrating flood-specific variables—including return-period inundation depth, population density, land cover classes, soil saturation, and additional environmental indicators—the study produces a national-scale flood risk map that can provide researchers and policymakers with a data-driven method for prioritizing flood mitigation infrastructure and improving future resilience.

- How can a flood risk assessment framework be designed to integrate diverse geospatial datasets—such as precipitation, hydrologic runoff, elevation, land cover, population density, and soil moisture—into a coherent, map-based classification of hazard, exposure, and vulnerability?
- What does combining these multidimensional datasets reveal about the advantages or limitation of the method compared to using mere flood inundation maps in flood risk analysis in Taiwan?

The central hypothesis of this work is that applying an integrated, WHO-inspired hazard–exposure–vulnerability framework—implemented using Google Earth Engine and open-source satellite datasets—will produce a more comprehensive and context-aware flood risk index for Taiwan than relying on traditional inundation maps or single-variable assessments in isolation.

## II. LITERATURE REVIEW

### A. WHO recommendation for calculating hazard risk

The WHO Guidance on Research Methods for Health Emergency and Disaster Risk Management recommends evaluating human health risks in disasters by examining three broad categories: Hazard, exposure, and vulnerability [5]. In this framework, the relationship used to calculate human risk is:

$$\text{Risk} = \text{Hazard} \times \text{Exposure} \times \text{Vulnerability}.$$

Hazard can be described by a particular disaster's location, severity, timing, duration, and frequency. These characteristics define the physical hazard itself. In flood risk classification, hazard may be measured by probability of flood reoccurrence at a given location which can be expressed through flood return periods or modeled inundation depth. In this study, the flood return periods will be used as accuracy and other factors such as precipitation data will help determine flood hazard.

Exposure can be described as the degree to which people or the environment will be impacted, directly or indirectly, by a particular disaster. This assesses the people who will be harmed by the physical hazard. In flood risk classification, exposure may be calculated by examining the population, level of human development, and or ecosystem that will be exposed to flooding which may be expressed through population density, critical infrastructure distribution, and evaluation of sensitive environmental areas.

Vulnerability and capacity can be described as the susceptibility and resilience of the people or the environment that will be impacted by the hazard. This assesses how severely people or environments would be impacted by flood. In flood risk classification, this could involve examining two contributors to susceptibility and resilience: human and environment. Human-related contributors may examine the population's knowledge of flood mitigation methods and the level of infrastructural and service preparedness for floods whereas environment-related contributors may examine the ability of the soil to absorb water, land use management, and other factors.

### B. Flood risk classification using Google Earth Engine

In a similar study to implement flood risk index mapping for Myanmar, research materials were derived from open datasets provided by the Department of Disaster Management Myanmar and the Google Earth Engine Python Application Programming Interface (API) [6]. The methodology used in the study calculated flood risk by considering the three WHO-recommended areas: hazard, exposure, and vulnerability. The final hazard index was based on the flood frequency values from JRC Global Water Dataset. The final exposure index combined multiple assets that would be impacted by flooding including population data from the 2015 World Population Dataset, land cover classification (particularly cropland, urban areas, and rice paddies) from the SERVIR-Mekong Land Cover Data, and critical distance data (particularly distances to roads, hospitals, and schools) from OpenStreetMap Contributors (2017). The final vulnerability index was based on

three socio-demographic values: age composition, literacy rates, and urbanization data from the Myanmar Department of Population. Due to dataset and local computational power restraints, this study took a similar approach to flood risk index mapping by taking advantage of the open-sourced data offered by Google Earth Engine Data Catalog and the cloud computing resources offered by Google Earth Engine Javascript Code editor.

## III. METHODOLOGY

### A. Materials

#### B. Case study: Taiwan

This study focuses on Taiwan, an island located along the Northwest Pacific tropical cyclone basin, at the western edge of the Pacific Ocean. Its terrain ranges from floodplains, to hills and plateaus, and to mountain ranges. Taiwan experiences heavy rainfall especially in the Mei-Yu season which starts mid-May and lasts until Mid-June. During this time, hot and humid air from the southwest converges with the cold and dry air from the north, causing air to rise and produce continuous rainfall, with average annual precipitation having been known to reach 2500 millimeters (mm). In the last century alone, there were more than 350 typhoons and 1000 rainfall events. In 2009, Typhoon Morakot accumulated 2777 mm within 3 days resulting in 677 deaths and \$3.3 billion USD in economic losses [4].

Taiwan flood hazard management is organized at the ministry, council, commission, and institutional levels in government. The Ministry of Economic Affairs (MOEA) implements policies for areas in between river embankments and their river basins through the central Water Resources Agency (WRA) and its ten regional River Administrations. The Ministry of Interior (MOI) is responsible for government flood mitigation and preventions in areas outside the active river basins. The MOI may advise county and city level governments to implement measures such as building stilt houses and rainwater harvesting systems, but ultimately city governments have final jurisdiction on implementing drainage and flood hazard preparedness policies. Currently, Taiwan's twenty-six largest rivers are protected against the reoccurrence of a 100-year flood event [4].

### C. Data

The Google Earth Engine Data Catalog provided the open-sourced datasets utilized in this study.

1) *Datasets for Hazard calculations:* The Climate Hazards Center InfraRed Precipitation with Station data (CHIRPS) provides a 5566-meters (m) per-pixel precipitation map, calculated daily from 1981-2025 0.05°-resolution satellite imagery combined with in-situ station data [7]. The precipitation variable represents millimeters (mm) of rain per day and was used for hazard index calculations.

The data suggested that urban centers around most of Taiwan's coastlines experience 500-mm of rain monthly with the exception of higher precipitation values nearly reaching 4000-mm in the southern coastlines.

The FLDAS Famine Early Warning Systems Network (FEWS NET) Land Data Assimilation System provides a 11,132-m or approximately 11-km per-pixel food security assessment map calculated from CHIRPS and Modern-Era Retrospective analysis for Research and Applications version 2 (MERRA-2) data [8]. The storm surface runoff variable in units of kilograms per meter squared per second, was used for hazard index calculations.

The NASA JPL's Shuttle Radar Topography Mission, SRTMGL1 V3 provides a 30-m per-pixel digital elevation map from the year 2000 [9]. The elevation variable represents the terrain height in meters above mean sea level and was also used to calculate other derived values such as slope and Terrain Wetness Index (TWI) for exposure index calculations.

The data suggested that elevation ranges were highly skewed in Taiwan with a mean value of 790.54-m, a median of 439.5-m, and a standard deviation of 845.96-m. The same can be said of derived slope values which range from 0° to 78.15° with a mean of 18.21° and a standard deviation of 14.58°. The TWI index, however, presents an even distribution with values ranging from 2.24 to 15.12 but mean and median being roughly equal and around 7.35 while the standard deviation is 1.15. Taiwan has high overall TWI values which indicated that the terrain is easily saturated and could lead to flooding.

*2) Datasets for Exposure calculations:* The European Space Agency (ESA) WorldCover 10m v200 data provides a 10-m per-pixel land cover map calculated from 2021 Sentinel-1 and Sentinel-2 data [10]. Out of the 11 land cover classes, this study focused on Cropland and Built-up classes for exposure index calculations.

The data suggested that the three dominant land cover classes in Taiwan were tree cover ( $\sim 29,414 \text{ km}^2$ ), cropland cover ( $\sim 3,750 \text{ km}^2$ ), and built-up reached ( $\sim 3,209 \text{ km}^2$ ).

**The WorldPop Global Project Population Data:** Estimated Residential Population per 100x100m Grid Square data provides a 92.77-m per-pixel population map calculated from 2000-2020 census population counts from their administrative units then divided the values into 92.77x92.77m grid cells through machine learning methods and random forest-based dasymetric redistribution [11]. The population variable represents the estimated number of people living in each grid cell and was used for exposure index calculations.

The 2020 data suggested that population density in Taiwan was highly skewed, with a median value of 0.57, a standard deviation of 21.5, a minimum of 0.004 and a maximum of 600.21. This reflects national settlement patterns, whereby the mountainous terrain that dominates the majority of the island is sparsely-populated, while the majority of the population are concentrated in urban centers along the coastlines and in northern part of Taiwan, particularly within the Taipei Basin, which are all regions with increased exposure to floods.

*3) Datasets for Vulnerability calculations:* The SPL4SMGP.008 SMAP L4 Global 3-hourly 9-km Surface and Root Zone Soil Moisture data provides a 11,000-m per-pixel soil moisture map [12]. The root-zone wetness variable represents 0-100cm soil moisture saturation on

a 0-1 scale and was used to calculate short-term flood vulnerability in vulnerability index calculations. The profile wetness variable describes the total soil moisture saturation down to the bedrock layer on a 0-1 scale and was used to calculate long-term flood vulnerability in vulnerability index calculations.

The data suggested that both the root-zone and profile wetness were highest in the northern regions of Taiwan including the area in the Taipei Basin with wetness values both reaching approximately 0.85. This could indicate that the region has a lower ability to saturate flood water compared to other regions.

*4) Dataset for reference:* The JRC Global River Flood Hazard Maps Version 2.1 provides a 90m per-pixel global river flood hazard map from March 16, 2024, for seven types of flood return periods (from 1-in-10-years to 1-in-500-years. The maps are computed by performing inundation simulations on the hydrological model LISFLOOD-FP. This map will be used for reference to compare the developed flood risk classification map with.

*5) Technology:* The Google Earth Engine JavaScript API was used to perform mapping and various calculations in this study. As a cloud-based platform, Google Earth Engine adopts the data-proximate computation model. Instead of downloading and storing petabytes of geospatial data locally, data-proximate computation brings the computational code to the data's location via the web-based JavaScript Code Editor which executes all necessary analyses within the cloud environment. This approach eliminates the need for extensive data transfer, storage, and processing.

#### D. Method

The methodology for computing the flood risk classification map were executed in the following sequential order:

- 1) Retrieve necessary variables from data
- 2) Re-project variables to a consistent resolution
- 3) Normalize variables
- 4) Compute flood risk index and classify
- 5) Compare classification with reference map

*1) Retrieve necessary variables from data:* Table I summarized the variables collected. Fig. 1. depicts each variable's raw spatial maps across Taiwan. Variables were selected from the latest available date, preferably from the year 2025.

Risk factor name	Variable used
Hazard	<ul style="list-style-type: none"> <li>• precipitation</li> <li>• storm surface runoff</li> <li>• elevation</li> <li>• slope</li> <li>• Terrain Wetness Index (TWI)</li> </ul>
Exposure	<ul style="list-style-type: none"> <li>• population</li> <li>• land cover classification (built-up and cropland specifically)</li> </ul>
Vulnerability	<ul style="list-style-type: none"> <li>• root zone soil wetness</li> <li>• profile soil wetness</li> </ul>

TABLE I

RISK FACTORS AND CORRESPONDING VARIABLE(S) FROM DATASET USED.

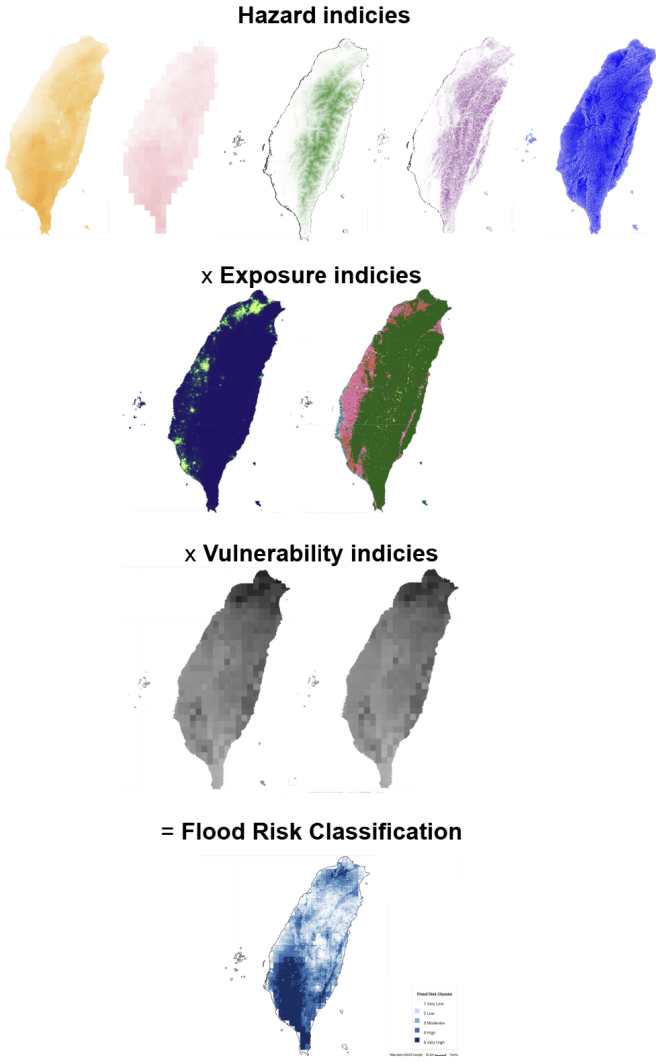


Fig. 1. Flood risk classification methodology

**2) Re-project variables to a consistent resolution:** For the multi-index analysis, variables with differing spatial resolutions were resampled and aggregated. This step involved setting each image's default projection to the target grid at a 150-m resolution. Up to 1,024 higher-resolution pixels were consolidated into a single output pixel. These parameters were selected based on computational limitations. Aggregation was then performed using the mean for continuous variables, the mode for categorical variables, and the sum for extensive variables. The resulting image was then re-projected to the target grid and projection.

**3) Normalize variables:** Normalization was applied to each variable to ensure consistency and comparability for subsequent steps in the methodology. Each variable was rescaled using min-max normalization so that the values were within the 0 to 1 range. The normalization formula was described as:

$$x_{\text{norm}} = \frac{x - x_{\min}}{x_{\max} - x_{\min}} \quad (1)$$

**4) Compute flood risk index and classify:** The variable values were multiplied by their corresponding weights then summed together to form continuous flood risk index values between 0 and 1. Weights for classification were assigned to the normalized variables as summarized in Table II. Variables representing Hazard were assigned the highest weights to reflect their primary contribution in flood occurrence likelihood. Among the Exposure variables, population received the greatest weight as it directly represents potential human exposure. Built-up land cover was weighted heavier than cropland given that populations are concentrated in built-up areas.

The resulting flood risk index values were then classified according to percentile thresholds at the 20th, 40th, 60th, or 80th percentiles.

Risk factor name	Variable used and weight
Hazard	<ul style="list-style-type: none"> <li>precipitation weight = 0.20</li> <li>storm surface runoff weight = 0.15</li> <li>elevation weight = 0.13</li> <li>slope weight = 0.13</li> <li>TWI weight = 0.15</li> </ul>
Exposure	<ul style="list-style-type: none"> <li>population weight = 0.10</li> <li>built-up land cover class weight = 0.04</li> <li>cropland land cover class weight = 0.02</li> </ul>
Vulnerability	<ul style="list-style-type: none"> <li>root zone soil wetness weight = 0.04</li> <li>profile soil wetness weight = 0.04</li> </ul>

TABLE II  
ASSIGNED WEIGHTS FOR VARIABLES.

**5) Compare classification with reference map:** The flood inundation depth for return period of 100 years from JRC Global River Flood Hazard Maps Version 2.1 were classified according to percentile thresholds at the 20th, 40th, 60th, or 80th percentiles. Fig. 2. shows the raw spatial map of flood inundation depth for return period of 100 years.

Confusion matrices, overall accuracies, kappa scores, producer's accuracies and user's accuracies were calculated.

#### IV. RESULTS

The predicted Very Low risk class accounts for 8,569.21- $\text{km}^2$  of area. The predicted Low risk class accounts for 6,872.90- $\text{km}^2$ . The predicted Moderate risk class accounts for 6,994.80- $\text{km}^2$ . The predicted High risk class accounts for 6,891.22- $\text{km}^2$ . The Very high risk class accounts for 6,798.99- $\text{km}^2$ .

In comparing the developed flood risk classification with the flood inundation depth for return period of 100 years from JRC Global River Flood Hazard Maps Version 2.1 on 03-16-2024, the overall accuracy score was 0.235, the kappa score was 0.00078. The producer's accuracy and user's accuracy scores are also listed in Fig. 5. The confusion matrix in Fig. 4. reveals limited agreement between the classes. The true data, flood inundation depth for return period of 100 years, is heavily imbalanced and around 95% of the data is classified as Very Low risk (1). Nevertheless, areas classified as Very High risk (5) show some correspondence with areas of high flood inundation depth (5).

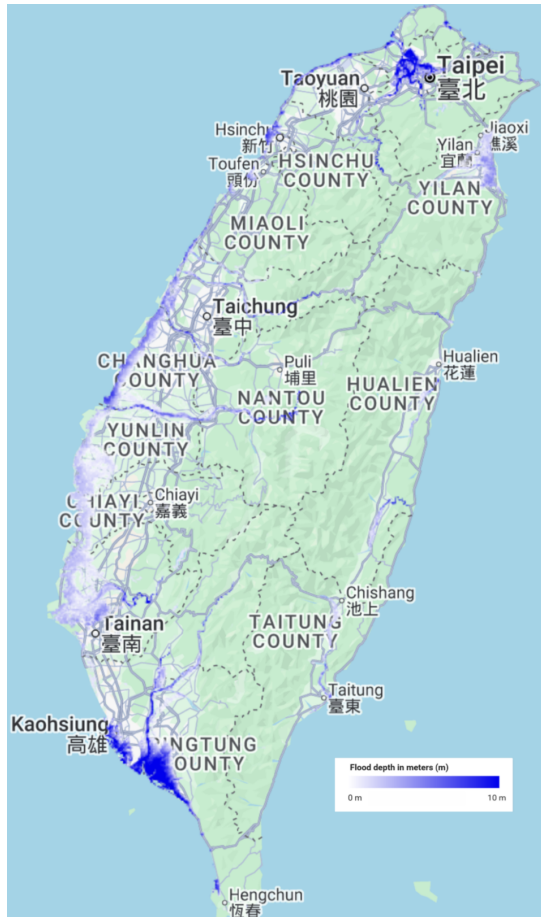


Fig. 2. Flood inundation depth for return period of 100 years from JRC Global River Flood Hazard Maps Version 2.1 on 03-16-2024

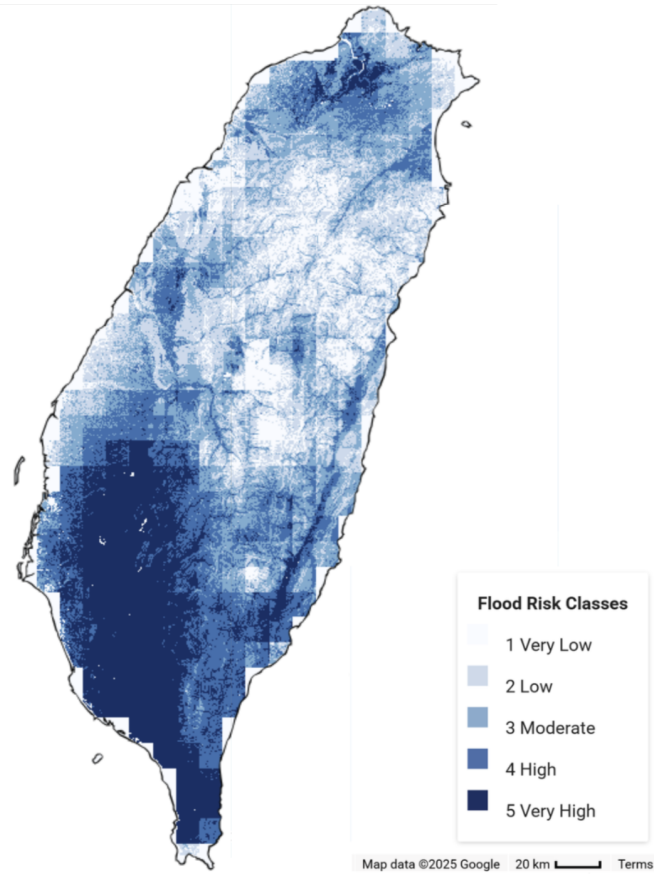


Fig. 3. Developed flood risk classification map

Additionally, when comparing the developed flood risk classification map in Fig. 3. and the raw flood inundation depth for return period of 100 years in Fig. 2., the maps show similar high intensities of either flood inundation depth or flood risk in the region below Kaohsiung, in Taipei Basin, and along the Hualien and Beinan River (between Hualien and Taitung).

The methodology developed in this paper addresses the first research question and presents how re-projection, resampling, aggregation (using mean, mode, or sum), and min-max normalization can integrate variables from diverse datasets together.

The results in this paper addresses the second research question by showing the advantages and limitations of using the developed flood risk classification framework. The advantage to the developed flood risk classification framework is that compared to raw flood inundation depth map, the developed flood risk classification is more detailed and it even classified the sparsely-populated mountainous regions. This addresses the need for floor risk classification in rural regions of the nation as mentioned in the literature review. The limitation of the method is that it can overestimate risk compared to the flood inundation depth classification.

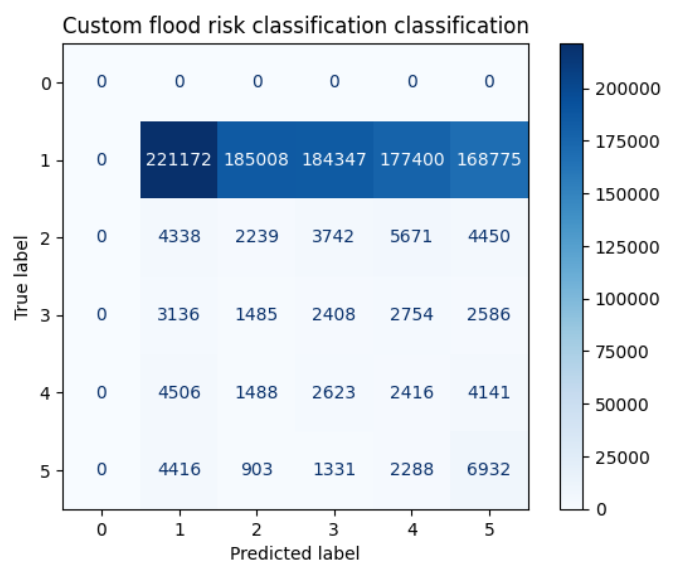


Fig. 4. Confusion matrix of flood risk classification versus Flood inundation depth for return period of 100 years

Overall accuracy: 0.23503655471213478

Kappa: 0.0007808654068986514

Class	Producer's Accuracy	User's Accuracy
0	0	0.000000
1	1	0.236118
2	2	0.109540
3	3	0.194680
4	4	0.159220
5	5	0.436799
		0.037093

Fig. 5. All accuracy-related scores of flood risk classification versus Flood inundation depth for return period of 100 years

## V. DISCUSSION

One contributor to the limitations in this study was the sparse flood-related dataset selection on Google Earth Engine Data Catalog. Not only were there few modern datasets to extract flood-related variables from, none of the datasets classified flood risk. This makes it difficult to convey any accuracy-related scores in the Results section of this paper because of the lack of true data. It should also be noted that traditionally, flood inundation depth for return periods are used as a variable for Hazard in flood risk classification, however, because of the lack of truth data limitation, it was used for the final evaluation as seen in the Results section of this paper.

The original objective was to use Random Forest for flood risk classification but since flood inundation depth is not truly indicative of flood risk as was found in the literature review, ultimately, the weights of each variable for risk classification were manually assigned.

Finally, due to some variables originating from extremely low-resolution datasets and the limited memory and computing power of Google Earth Engine JavaScript API, a finer-resolution risk classification map could not be achieved for this study.

The methodology already provides a flexible foundation for future flood risk studies and can be enhanced through adjusting weighting schemes, adding socio-economic variables as Vulnerability factor, or validating against event-based flood observations.

## VI. CONCLUSION

This study developed a national-scale flood risk index for Taiwan by integrating hazard, exposure, and vulnerability components within the World Health Organization's disaster risk framework using Google Earth Engine and open-source geospatial datasets. The proposed methodology demonstrates a practical and computationally-efficient approach for combining variables of differing resolutions such as precipitation, hydrologic runoff, topography, land cover, population density,

and soil moisture into a flood risk classification map through re-projection, resampling, aggregation, and min–max normalization.

The resulting flood risk map provides a comprehensive representation of flood risk compared to traditional flood inundation depth alone by incorporating exposure and vulnerability-related variables with hydraulic hazard-variables. While the comparison with the JRC 100-year flood inundation depth map revealed limited overall agreement—reflected by low overall accuracy and kappa values—this outcome can be caused by the differences between a relative flood risk index and a scenario-based flood hazard product and the strong class imbalance in the reference data.

However, more importantly, areas classified as Very High risk aligned with regions of high modeled flood inundation depth, including southern Taiwan near Kaohsiung, the Taipei Basin, and major river corridors in eastern Taiwan, indicating that the developed index did capture certain meaningful flood-related patterns.

The findings showcases both the strengths and limitations of the proposed framework. Compared to raw inundation maps, the flood risk classification offers enhanced spatial detail and accounts for population and environmental vulnerability, allowing for risk identification in both urban centers and sparsely-populated mountainous regions. However, exposure or vulnerability factors may inflate flood risk despite flood inundation depth indicating the area as having Very low or Low risk for flood.

As climate change continues to intensify flood devastation in Taiwan, comprehensive risk-based approaches such as the one developed in this paper can inform flood mitigation planning, update infrastructure prioritization, and improve long-term resilience strategies.

## VII. FIGURES



Fig. 6. The 5 hazard-related variables. (view in GitHub)

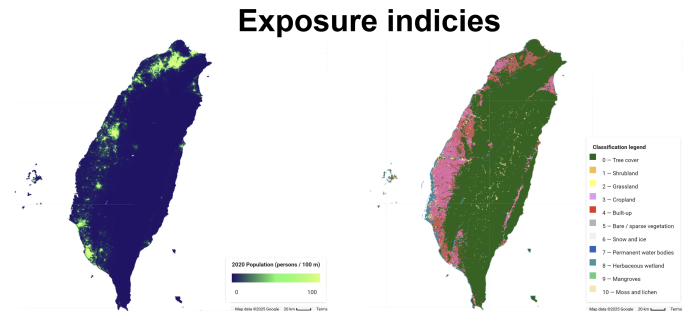


Fig. 7. The 2 exposure-related variables

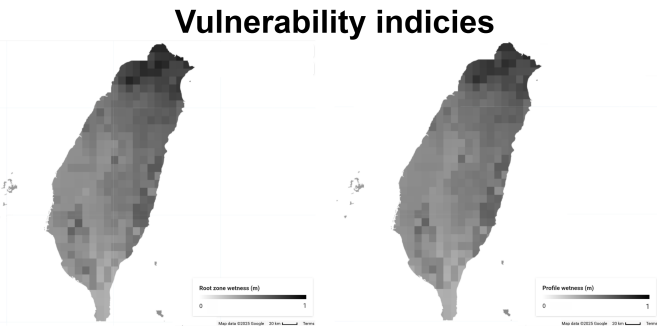


Fig. 8. The 2 vulnerability-related variables

## REFERENCES

- [1] Y.-H. Hsiao, C.-C. Chen, Y.-C. Chao, H.-C. Li, C.-H. Ho, C.-T. Hsu, and K.-C. Yeh, "Development and application of flood impact maps under climate change scenarios: A case study of the yilan area of Taiwan," *Frontiers in Environmental Science*, vol. 10, Sep. 2022 [Online]. Available: <https://www.frontiersin.org/journals/environmental-science/articles/10.3389/fenvs.2022.971609/full>. [Accessed: 08-Dec-2025]
- [2] . Huang, T. Lee, C. Lin, Y. Lin, and H. Hsu, "Impacts of global warming on severe drought in northern Taiwan: A future projection based on the year 2021," *International Journal of Climatology*, vol. 45, no. 14, Aug. 2025 [Online]. Available: <https://rmets.onlinelibrary.wiley.com/doi/10.1002/joc.70094>. [Accessed: 08-Dec-2025]
- [3] S.-C. Huang, W.-R. Huang, Y. Wu, Y.-C. Yu, J.-L. Chu, and B. J.-D. Jou, "Characteristics and causes of Taiwan's extreme rainfall in 2022 January and February," *Weather and Climate Extremes*, vol. 38, p. 100532, Dec. 2022 [Online]. Available: <https://www.sciencedirect.com/science/article/pii/S2212094722001116>. [Accessed: 08-Dec-2025]
- [4] H.-W. Wang, D. S. Castillo Castro, and G.-W. Chen, "Managing residual flood risk: Lessons learned from experiences in Taiwan," *Progress in Disaster Science*, vol. 23, p. 100337, Oct. 2024 [Online]. Available: <https://www.sciencedirect.com/science/article/pii/S2590061724000279>. [Accessed: 08-Dec-2025]
- [5] World Health Organization, WHO guidance on research methods for health emergency and disaster risk management, revised 2022. Genève, Switzerland: World Health Organization, 2022.
- [6] K. Phongsapan, F. Chishtie, A. Poortinga, B. Bhandari, C. Meechaiya, T. Kunlamai, K. S. Aung, D. Saah, E. Anderson, K. Markert, A. Markert, and P. Towashiraporn, "Operational flood risk index mapping for disaster risk reduction using earth observations and cloud computing technologies: A case study on Myanmar," *Frontiers in Environmental Science*, vol. 7, Dec. 2019 [Online]. Available: <https://www.frontiersin.org/journals/environmental-science/articles/10.3389/fenvs.2019.00191/full>. [Accessed: 08-Dec-2025]
- [7] C. Funk, P. Peterson, M. Landsfeld, D. Pedreros, J. Verdin, S. Shukla, G. Husak, J. Rowland, L. Harrison, A. Hoell, and J. Michaelsen, "The climate hazards infrared precipitation with stations—a new environmental record for monitoring extremes," *Scientific Data*, vol. 2, no. 1, Dec. 2015 [Online]. Available: <https://www.nature.com/articles/sdata201566>. [Accessed: 08-Dec-2025]
- [8] Amy McNally, "FLDAS Noah Land Surface Model L4 Global Monthly 0.1 x 0.1 degree (MERRA-2 and CHIRPS)", Greenbelt, MD, USA, Goddard Earth Sciences Data and Information Services Center (GES DISC), NASA/GSFC/HSL, 2018. Available: [https://disc.gsfc.nasa.gov/datasets/FLDAS\\_NOAH01\\_C\\_GL\\_M\\_001/summary](https://disc.gsfc.nasa.gov/datasets/FLDAS_NOAH01_C_GL_M_001/summary). [Accessed: 08-Dec-2025]
- [9] T. G. Farr, P. A. Rosen, E. Caro, R. Crippen, R. Duren, S. Hensley, M. Kobrick, M. Paller, E. Rodriguez, L. Roth, D. Seal, S. Shaffer, J. Shimada, J. Umland, M. Werner, M. Oskin, D. Burbank, and D. Alsdorf, "The shuttle radar topography mission," *Reviews of Geophysics*, vol. 45, no. 2, May 2007 [Online]. Available: <https://agupubs.onlinelibrary.wiley.com/doi/10.1029/2005RG000183>
- [10] D. Zanaga, "ESA WorldCover 10 m 2021 v200", Zenodo, Oct. 28, 2022. doi: 10.5281/zenodo.7254221. [Online]. Available: <https://zenodo.org/records/7254221>. [Accessed: 08-Dec-2025]
- [11] A. Sorichetta, G. M. Hornby, F. R. Stevens, A. E. Gaughan, C. Linard, and A. J. Tatem, "High-resolution gridded population datasets for Latin America and the Caribbean in 2010, 2015, and 2020," *Scientific Data*, vol. 2, no. 1, Sep. 2015 [Online]. Available: <https://www.nature.com/articles/sdata201545>. [Accessed: 08-Dec-2025]
- [12] R. Reichle et al., "SMAP L4 Global 3-hourly 9 km EASE-Grid Surface and Root Zone Soil Moisture Geophysical Data, Version 8," NASA National Snow and Ice Data Center Distributed Active Archive Center, 2025. doi: 10.5067/T5RUATAQREF8. Available: <https://nsidc.org/data/spl4smgp/versions/8>